7th US National Technical Meeting of the Combustion Institute
Hosted by the Georgia Institute of Technology, Atlanta, GA
March 20-23, 2011

A Comparative Study of the Sooting Properties of Laminar Premixed Flames of C_6 Hydrocarbons

Joaquin Camacho, Sydnie Lieb and Hai Wang

Department of Aerospace and Mechanical Engineering,
University of Southern California, Los Angeles, California 90089-1453, USA

The effect of fuel structure on global and detailed sooting processes is examined by measuring detailed particle size distribution functions (PSDF) of nascent soot formed in a set of canonical, laminar premixed flames of C_6 hydrocarbons. Specifically, the evolution of the PSDFs in benzene, *n*-Hexane and cyclohexane flames were determined at C/O ratio of 0.69 and maximum flame temperatures of 1800K and 2000K. To assist in data interpretation, comparable ethylene flames were also included in the experimentation. At maximum flame temperatures of 2000K, the analyses demonstrate that properties such as volume fraction and particle size are dependent upon fuel structure quite strongly, whereas these properties are nearly identical for the fuels at maximum flame temperature of 1800K.

1. Introduction

Soot formation is a kinetic process of combustion that is integral to the optimization of any combustion device. Practical fuels such as gasoline and biodiesel are complex mixtures of hydrocarbons and organics therefore, a direct kinetic description of their combustion behavior, including soot formation, is not feasible due to the variability and complex nature of the mixtures. However, the study of combustion behavior for fuel surrogates is regularly carried out to better understand the behavior of practical fuels [1, 2]. In recent years, efforts have been directed at developing combustion reaction models for fuel surrogates and the natural progression of such models requires the inclusion of higher PAH and soot chemistry [3]. Eventually, greater complexity will be required to model phenomena other than fundamental properties such as ignition delay or laminar flame speed [1]. In order to progress soot chemistry, a systematic approach must be taken to understand the interplay between the governing parameters of soot formation such as the local flame temperature and equivalence ratio.

The present work aims to investigate soot formation in premixed laminar n-hexane, cyclohexane,

and benzene flames with an emphasis on the evolution of the detailed particle size distribution function (PSDF). The sooting behavior is measured at the same maximum flame temperature and carbon to oxygen ratio so that the effect of the parent fuel structure upon soot formation can be isolated. The effect of flame temperature on sooting premixed burner-stabilized flames has been carried out for various fuels but a systematic cross comparison of the temperature effects for different fuels does not exist [4, 5]. Various experiments and modeling have been carried out on sooting benzene, cyclohexane and *n*-hexane flames but the effect of flame temperature was not completely eliminated across the fuels studied [6-9]. In the present work, the sooting behavior of the parent fuel was studied at a maximum flame temperature of 1800K and 2000K. The burner stabilized stagnation flame method (BSS); described in detail elsewhere [10, 11]; was employed to investigate the evolution of size distribution in nascent soot from the particle nucleation stage to mass growth. The method allows for intrusive soot sampling while directly accounting for probe obstruction to the flame. A conventional burner stabilized flame is subjected to flow stagnation and probe sampling simultaneously such that the temperature at the top of the flame can be rigorously defined as a boundary condition in reacting flow simulations. With the flow field defined, the flame temperature and species concentrations up to lower PAHs can be directly modeled using a quasi-one dimensional opposed jet code without imposing a measured temperature profile or correcting for artificial probe perturbation [10]. The model allows for premixed flames BSS flames to be calculated at the same maximum flame temperature for a given C/O ratio without the need for preliminary temperature measurements.

2. Experimental Methodologies

The BSS flame approach; described in detail elsewhere [10, 11]; has been extended to the aforementioned C_6 hydrocarbons. The BSS flame configuration can be simulated directly as a reacting flow because the sampling probe simultaneously acts as stagnation surface with a well defined boundary temperature. Eight lightly sooting flames were stabilized in the BSS flame configuration at atmospheric pressure with maximum flame temperatures of 1800K and 2000K (Table 1). The liquid fuels were vaporized and injected into the fuel line in a manner similar to previous studies [11]. The burner size has been reduced to 5 cm at the fuel inlet to increase the range of possible flame temperatures and to increase the lifetime of the sintered bronze material that the flame is stabilized over. The flat flame burner is not water cooled during liquid fuel experiments, thus the upper porous material surface is subjected to temperatures which close the pores and change the flame conditions. Fresh porous material was always used to keep the flame roughly one dimensional. At probe separation distances above 1.5 cm, a burner diameter of 7.6 cm was employed to maintain a 1-D flame condition. The mass flow rates of oxygen, argon and nitrogen are

measured by critical orifices and the flow of argon driving the fuel nebulizer was calibrated by bubble displacement. The gas temperature profiles were measured with a coated Type-S thermocouple and radiation correction to the thermocouple was carried out numerically in a procedure that is discussed earlier [11].

Particle size distributions were measured with a standard TSI SMPS/CPC setup [10]. The flame gas entered the probe through the orifice and was immediately diluted with a cold nitrogen flow to prevent particle losses. The dilution range and calibration has been used before and care was taken to avoid diffusion losses, condensation of higher PAHs, and probe-induced coagulation during dilution [4]. Limitations to the Cunningham slip correction cause particles below 10 nm to be overestimated by mobility measurements and thus a nano-particle transport theory was used for small particles to obtain more accurate particles sizes [12-14].

The experimentally measured temperature profiles are radiation corrected by using transport and flow properties that are calculated by a modified version of OPPDIF [10]. The probe separation to plate diameter ratio is much less than unity so the quasi 1-D assumption applies. The flame chemistry is calculated with JetSurF (version 2.0) [3]. By energy conservation, the modified OPPIF code allows for the calculation of the temperature and species profile without the need for a measured temperature profile as an input. The radiation corrected temperature profiles are compared to the calculated OPPDIF profile to test the validity of the experimental and numerical procedures. The inlet fuel temperature was extrapolated from the measured temperature profile and the probe temperature was measured with a type K thermocouple embedded on the stagnation surface. The flame conditions are summarized in Table 1. Each of the four fuels was studied at C/O = 0.69 and maximum flame temperatures of 1800K and 2000K.

Table 1. Summary of the premixed flame compositions

Mole fractions						
C_2H_4	O_2	Ar	C/O ratio	Equivalence ratio, ϕ	Velocity, v_o (cm/s)	Flame temperature, $T_{f,max}$ (K)
0.1620	0.2345	0.6036	0.69	2.07	7.47	1800
0.1626	0.2353	0.6020	0.69	2.07	15.48	2000
C_6H_6	O_2	Ar				
0.0441	0.1913	0.7645	0.69	1.73	4.43	1800
0.0395	0.1693	0.7913	0.70	1.75	10.04	2000
C_6H_{12}	O_2	Ar				
0.0742	0.3224	0.6034	0.69	2.07	3.77	1800
0.0741	0.3217	0.6042	0.69	2.07	8.33	2000
n-C_6H_{14}	O_2	Ar				
0.0737	0.3206	0.6057	0.69	2.18	4.62	1800
0.0739	0.3211	0.6050	0.69	2.19	10.71	2000

[a] STP condition. [b] Corrected for radiation heat loss.

3. Results and Discussion

The BSS flame configuration yields a different flame for each burner to probe separation distance, H_p. The degree to which flow divergence and heat loss affects the temperature profiles as H_p increases is shown in Figure 1 for a series *n*-hexane flames with maximum flame temperatures of 1800K and benzene flames at 2000K. At both temperatures, the agreement between radiation corrected measurements and simulated temperatures is within thermocouple positioning uncertainty of ±0.03 cm and ±70 K for temperature. The position of the thermocouple is affected by the tension of the wire and other factors and the emissivity of the thermocouple during measurements is assumed to be between 0.3 and 0.6 [15].The simulation predicts slightly higher temperatures than measured within regions of the pre-flame and post-flame. The agreement exhibited in Figure 1 is similar for ethylene and cyclohexane flames at both temperatures used in this study.

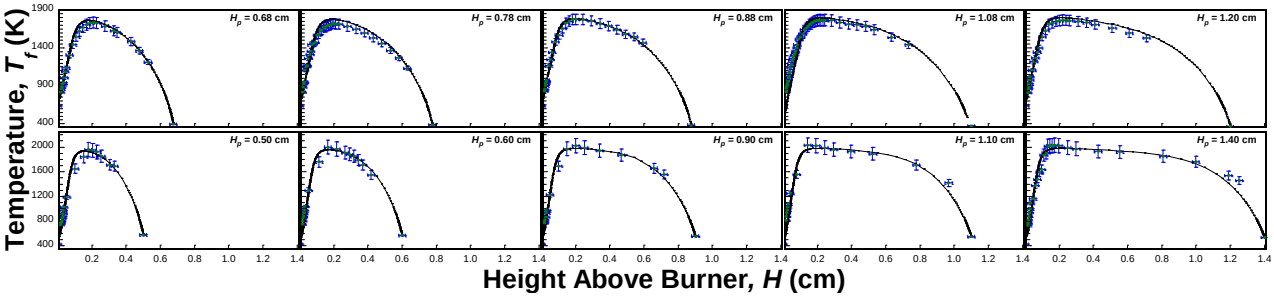

Figure 1: Comparison of temperature profiles for measurements (symbols, radiation corrected) and simulation (lines) for *n*-hexane flames at $T_{f,max}$ = 1800K (top row) and benzene flames at $T_{f,max}$ = 2000K (bottom row). The profiles were simulated with a modified version of OPPDIF which utilized JetSurF 2.0 flame chemistry [3].

The OPPDIF model solves the energy equation without the measured temperature profiles as an input. Thus, agreement between radiation corrected measurements and the simulation addresses uncertainty within the JetSurF mechanism itself by yielding information on local heat release and loss rates [11]. Such information allows for the uncertainty within the simulated local temperature to be defined along with the resulting Arrhenius reaction kinetics and species transport. Furthermore, the agreement in measured temperures and the model confirms that each flame temperature is either 1800K or 2000K and the effect of fuel structure is isolated from temperature effects.

Detailed PSDF were measured for each of the lightly sooting flames from nucleation to mass growth. A representative example of the evolution of the PSDF is given in Figure 2 as series of *n*-hexane flames at both respective flame temperatures. The detailed distributions provide insight into

the competitive processes such as nucleation, coagulation and surface growth. Such processes are heavily dependent upon temperature therefore deeper insight is obtained by observing more than one temperature regime. In each of the 1800K flames, the lack of fragmentation of soot precursors allowed for steady nucleation of soot in a fashion that was similar for each fuel. At the lower temperature, less fragmentation occurs and the soot mass continues to grow in a similar manner for each fuel studied. This leads to PSDFs which assume a bimodal distribution containing a prominent nucleation tail that exists well into the post-flame region.

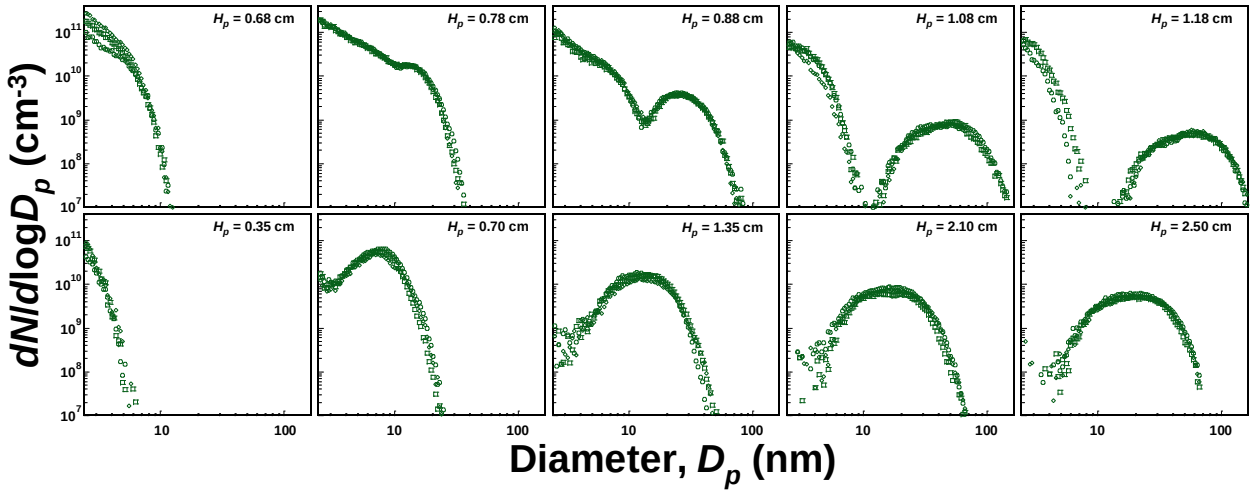

Figure 2: PSDFs measured for the *n*-hexane flames at maximum flame temperatures of 1800K (top row) and 2000K (bottom row).

The persistent nucleation tail and strong coagulation mode shown in Figure 2 also represents the features of the detailed PSDF measured for ethylene, benzene and cyclohexane flames at 1800K. In fact, all of the lower temperature flames studies exhibited PSDFs that were similar to previous measurements of ethylene and dodecane at comparable flame conditions [10, 11]. As expected, Figure 2 shows that the 2000K flames are in an environment where soot nucleates earlier due to faster Arrhenius kinetics while the thermodynamic reversibility of fragmentation limits the mass growth process [11]. However, the present work aims to isolate the effect of the parent fuel structure upon soot formation therefore a comparison across each fuel is required as the PSDF is studied across the temperature regimes.

A summary of the effect upon the detailed PSDF for each fuel at each temperature regime is shown is Figure 3. The lower temperature regime is characterized by a strong nucleation tail and mass growth mode as discussed in Figure 2. The details of the PSDF are almost identical for the 1800K flames hence the competing kinetic processes in soot formation are similar under such conditions. The parent fuel structure seems to have little effect upon the sooting behavior of the C_6 hydrocarbons with C/O ratio of 0.69 and maximum flame temperature of 1800K. On the other hand,

each of the higher temperature flames show diverse details within the PSDF as the flame temperature is raised. The diverse response to temperature within the PSDF indicates that overall mechanism of soot formation changes in a fuel dependent manner. At the lower temperature, the persistent bimodal distribution implies that mass growth is limited by the amount of freshly nucleated particles available for coagulation. That is, dominant driving force of soot growth is not sensitive to fuel structure at the given temperature.

The diversity in PSDF features at the higher temperature reveals a more complex situation. For example, the sooting propensity of cyclohexane diverges from ethylene and benzene at higher temperatures even though the C/O and C/H ratio are the same or comparable. Pure benzene flames may not be comparable at C/O =0.69 because there is significantly less excess fuel. Comparable benzene flame measurements may require H_2 doping or a compensation in equivalence ratio. However, the variation median diameter shift shown in Figure 3 can be attributed to fuel structure for ethylene, cyclohexane and *n*-hexane flames.

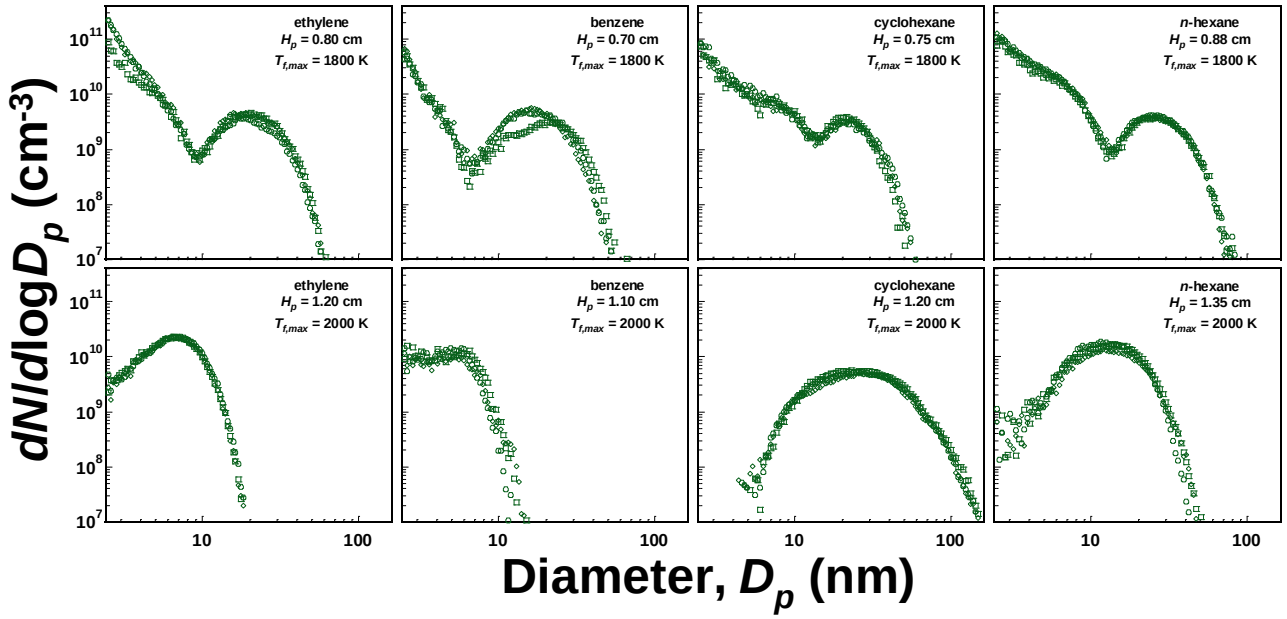

Figure 3: Shift in the PSDF of ethylene and the C_6 hydrocarbons as the maximum flame temperature increases from 1800K (top row) to 2000K (bottom row).

For a given sampling height and soot density, the integration of the detailed PSDF yields the total soot volume fraction. The global sooting characteristics for each BSS flame are summarized in terms of the total volume fraction in Figure 4. For each series of flames, the volume fraction is seen to approach an asymptotic value where a balance between soot formation and fragmentation occurs. The global behavior of ethylene and the C_6 hydrocarbons is the same at the lower temperature condition as discussed earlier. However, the PSDF shifts for each flame as the maximum flame temperature is increased in a manner that depends upon the structure of the parent fuel. Flames from

aromatic fuels are known soot more readily than straight chain at a given C/O ratio. However, the relatively low benzene flame volume fraction shown in Figure 3 indicates that fragmentation of soot precursors may dominate at flame temperatures of 2000K. The relative disparity in excess fuel between benzene (ϕ = 1.7) and the other flames (ϕ = 2) may be the dominating factor which allows inhibits soot formation at the higher flame temperature. As discussed in Figure 2, the overall carbon and hydrogen ratios of ethylene, cyclohexane and *n*-hexane are comparable. At the higher temperature condition, Figure 4 shows that the cyclic functional group allows for a greater volume fraction than the straight chain isomer. The ethylene fuel is not a representative for the alkene functional group and however, future work must be carried out on hexene for such a comparison.

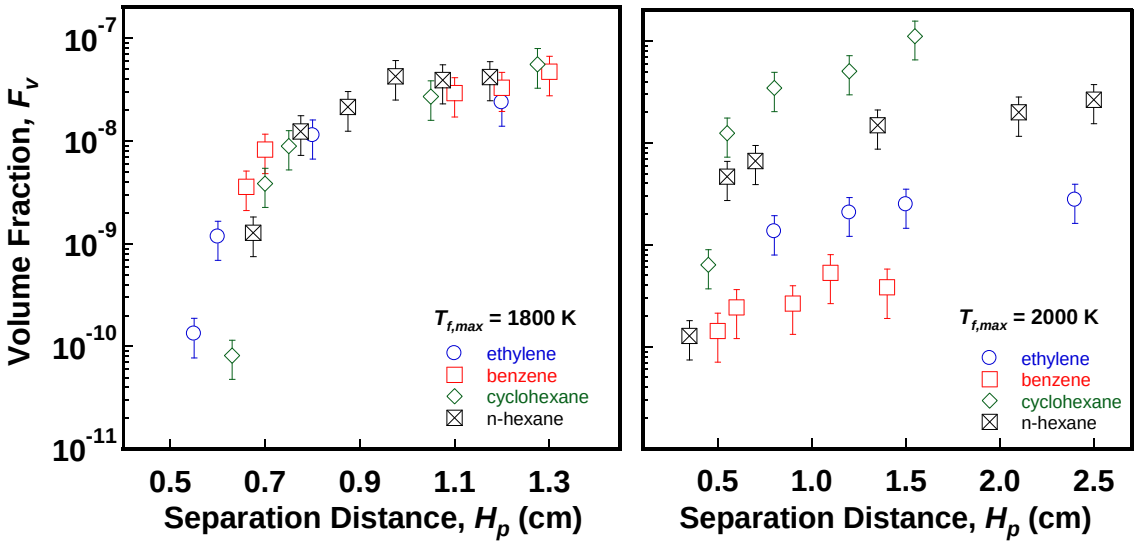

Figure 4: Total volume fraction measured at several H_p for ethylene and the C_6 hydrocarbons at C/O = 0.69 and maximum flame temperatures of 1800K and 2000K.

4. Conclusions

The PSDF measurements of these C_6 hydrocarbon flames with maximum flame temperature of 2000K demonstrated diverse details within the measured PSDF. On the other hand, measurements of the lower temperature flames showed nearly identical global and detailed sooting properties across all flames studied. In the future, a deeper fundamental understanding of competitive soot processes and the impact of fuel structure on these processes is required.

5. Acknowledgements

The work was supported in part by the National Science Foundation (CBET 0651990) and by the Combustion Energy Frontier Research Center (CEFRC), an Energy Frontier Research Center funded

by the U.S. Department of Energy, Office of Science, Office of Basic Energy Sciences under Award Number DE-SC0001198.

6. References

1. H. Wang, *Proceedings of the Combustion Institute* 33, 41-67.
2. M. Colket; J. T. Edwards; S. Williams; N. P. Cernansky; D. L. Miller; F. N. Egolfopoulos; P. Lindstedt; K. Seshadri; F. L. Dryer; C. K. Law; D. G. Friend; D. B. Lenhert; H. Pitsch; A. F. Sarofim; M. D. Smooke; W. Tsang, in: *45th AIAA Aerospace Sciences Meeting, Jan 8-11*, Reno, NV, 2007; AIAA Paper 2007-0770.
3. B. Sirjean; E. Dames; D. A. Sheen; X. You; C. J. Sung; A. T. Holley; F. N. Egolfopoulos; H. Wang; S. S. Vasu; D. F. Davidson; R. K. Hanson; H. Pitsch; C. T. Bowman; A. Kelley; C. K. Law; W. Tsang; N. P. Cernansky; D. Miller; A. Violi; R. P. Lindstedt A high-temperature chemical kinetic model of n-alkane (up to n-dodecane), cyclohexane, and methyl-, ethyl-, n-propyl and n-butyl-cyclohexane oxidation at high temperatures, JetSurF version 2.0, September 19, 2010 (http://melchior.usc.edu/JetSurF/JetSurF2.0).
4. A. D. Abid; N. Heinz; E. Tolmachoff; D. Phares; C. Campbell; H. Wang, *Combustion and Flame* **2008,** 154, 775-788.
5. M. Alfe; B. Apicella; J. N. Rouzaud; A. Tregrossi; A. Ciajolo, *Combustion and Flame* 157, 1959-1965.
6. C. A. Echavarria; A. F. Sarofim; J. S. Lighty; A. D'Anna, *Proceedings of the Combustion Institute* **2009,** 32, 705-711.
7. C. A. Echavarria; A. F. Sarofim; J. S. Lighty; A. D'Anna, *Combustion and Flame* 158, 98-104.
8. A. Ciajolo; A. Tregrossi; M. Mallardo; T. Faravelli; E. Ranzi, *Proceedings of the Combustion Institute* **2009,** 32, 585-591.
9. M. Alfè; B. Apicella; R. Barbella; A. Tregrossi; A. Ciajolo, *Proceedings of the Combustion Institute* **2007,** 31, 585-591.
10. A. D. Abid; J. Camacho; D. A. Sheen; H. Wang, *Combustion and Flame* **2009,** 156, 1862-1870.
11. A. D. Abid; J. Camacho; D. A. Sheen; H. Wang, *Energy & Fuels* **2009,** 23, 4286-4294.
12. Z. Li; H. Wang, *Journal of Aerosol Science* **2006,** 37, 111-114.
13. Z. G. Li; H. Wang, *Physical Review E* **2003,** 68.
14. Z. G. Li; H. Wang, *Physical Review E* **2003,** 68.
15. R. C. Peterson; N. M. Laurendeau, *Combustion and Flame* **1985,** 60, 279-284.